

Quantum Gradient Algorithm for General Polynomials

Keren Li,^{1,2,*} Pan Gao,^{1,*} Shijie Wei,^{3,1} Jiancun Gao,¹ and Guilu Long^{1,4,3,5,†}

¹*State Key Laboratory of Low-Dimensional Quantum Physics and
Department of Physics, Tsinghua University, Beijing 100084, China*

²*Center for Quantum Computing, Peng Cheng Laboratory, Shenzhen 518055, China*

³*Beijing Academy of Quantum Information Sciences, Beijing 100193, China*

⁴*Beijing National Research Center for Information Science and Technology
and School of Information Tsinghua University, Beijing 100084, China*

⁵*Frontier Science Center for Quantum Information, Beijing 100084, China*

(Dated: April 24, 2020)

Gradient-based algorithms, popular strategies to optimization problems, are essential for many modern machine-learning techniques. Theoretically, extreme points of certain cost functions can be found iteratively along the directions of the gradient. The time required to calculating the gradient of d -dimensional problems is at a level of $\mathcal{O}(\text{poly}(d))$, which could be boosted by quantum techniques, benefiting the high-dimensional data processing, especially the modern machine-learning engineering with the number of optimized parameters being in billions. Here, we propose a quantum gradient algorithm for optimizing general polynomials with the dressed amplitude encoding, aiming at solving fast-convergence polynomials problems within both time and memory consumption in $\mathcal{O}(\text{poly}(\log d))$. Furthermore, numerical simulations are carried out to inspect the performance of this protocol by considering the noises or perturbations from initialization, operation and truncation. For the potential values in high-dimension optimizations, this quantum gradient algorithm is supposed to facilitate the polynomial-optimizations, being a subroutine for future practical quantum computer.

INTRODUCTION

Recent advances indicate that machine learning (ML) methods is coming into prominence as the potential solutions to various challenging physical problems, such as identification of phases of matter[1, 2], representation of many-body states[3, 4] and quantum entanglement, tomography[5–7]. Gradient-based algorithms, consisting of the prototypical gradient method and its variants, are essential to many optimization problems, which are the keys to most ML methods. They are extensively applied to logistic regression, support vector machine, neural network and those whose inside parameters are to be optimized[8–11]. With the advent of vigorous machine-learning (ML) methods, which have been ubiquitously powering the modern technologies[12–14], ML methods are destined to process an incredible amount of data generated in this internet era. Although, the time required to calculating the gradient of d -dimensional problems is at a level of $\mathcal{O}(\text{poly}(d))$. For the modern architecture, the number of parameters to be optimized would be in billions. Calculating such a scale of gradient would be computationally intractable.

Though to-date quantum computing engineering is still on a modest stage which is far to meet the requirements of practical quantum computing, dramatic hardware improvements has been achieved for decades in both the scale and the quality of qubits[15, 16]. It offers a tantalizing prospect to outperform the most powerful electronic computer[17], providing an exponential speed-up for certain problems[18, 19]. Many quantum enhanced algorithms are emerging, such as quantum Fourier transformation (QFT)[17], *HHL* linear

equation algorithm[20] and quantum principle component analysis (qPCA)[21]. As for enhancing the gradient-based algorithms, plenty of research on their quantum version has been published[22–27]. However, as their different applicable conditions, a general quantum gradient algorithm is still required.

As polynomials can not only be directly applied into some ML models but also be approximation of arbitrary functions[28, 29], in this paper, we propose a quantum gradient algorithm correspondingly based on the previous framework[26]. The dressed amplitude encoding (DAE) method and a non-unitary subroutine are introduced, realizing the calculation on the gradient of general polynomials which is no more homogeneous and even order. As constrained optimization problems usually can be transformed into unconstrained optimization problems by introducing penalty function or Lagrange method, our protocol, dropping the constraints on feasible points, extends the framework to more optimization cases. Besides, numerical simulations are conducted within consideration of noise or perturbations for both maximum and minimum problems. Although it would be more applicable in fast convergence problems due to the finite success probability and the multi-copies required for each iteration. By the results, our adapted protocol shows the robustness to experiment concerned errors of reasonable strengths, which is important for the real application in Noisy Intermediate-Scale Quantum (NISQ) computers. Moreover, the protocol inherits the advantage of the amplitude encoding that reducing both memory and time consumption to $\mathcal{O}(\text{poly} \log d)$. As the importance of high dimensional optimization problems in modern machine-learning methods, this algorithm have the potential to

boost the interdisciplinary research of quantum computing and machine-learning.

RESULT

Maximizing or minimizing $f(\mathbf{x})$, where \mathbf{x} is a d -dimensional real variable $(x_1, x_2, \dots, x_d)^T$, is a prototypical optimization problem and gradient-based algorithms are usually resorted to. Let ξ be the learning rate and superscript t stands for the iteration steps, the variable thus can be updated iteratively with

$$\mathbf{x}^{t+1} = \mathbf{x}^t \pm \xi \nabla f(\mathbf{x}^t). \quad (1)$$

where $+$ ($-$) corresponds to the maximum(minimum) problem. To be noticed, all the superscript(and subscript) denoting step index and variable will be omitted in remaining text.

Protocol—General polynomials optimization with no more than $2p$ -order is considered in this paper. By introducing $\mathbf{X} = (1, \mathbf{x}^T)^T$, polynomial cost function can be written as

$$f(\mathbf{X}) = \frac{1}{2} \mathbf{X}^{T \otimes p} A \mathbf{X}^{\otimes p} \quad (2)$$

where A is a $(d+1)^p \times (d+1)^p$ matrix which specifies the coefficient of polynomials. Inasmuch as complex number can be treated as two independent real ones, and global scaling of f cause no impact on the extreme points, A can always be chosen as real symmetric and scaled as $A \sim A/p||A||_{max}$ for convenience of following analysis.

The corresponding gradient ∇f can be expressed as a part of $\hat{D}\mathbf{X}$ as

$$\left(\begin{smallmatrix} \kappa \\ \nabla f \end{smallmatrix} \right) = \left[\mathbf{X}^{T \otimes p-1} \sum_{k=1}^p P_k A P_k^\dagger \mathbf{X}^{\otimes p-1} \right] \mathbf{X} \equiv \hat{D}\mathbf{X}, \quad (3)$$

where P_k is the permutation operator, swapping the 1-st and the k -th $(d+1) \times (d+1)$ subspaces in A . Thus $\hat{D} = \mathbf{X}^{T \otimes p-1} \sum_{k=1}^p P_k A P_k^\dagger \mathbf{X}^{\otimes p-1}$ is dubbed as a variable dependent gradient operation. Noticeably, κ is redundant and is to be cast away to export a right ∇f with the expression of \hat{D} .

Therefore, Eq.(2) and Eq.(3) establish the depiction of the polynomials optimization. As for its quantum version, a dressed amplitude encoding(DAE) method introduced as

$$\mathbf{X} \rightarrow |\mathbf{X}\rangle = \cos \gamma (|0\rangle + \sum_{i=1}^d x_i |i\rangle), \quad (4)$$

with the \mathbf{x} -dependent normalization factor $\cos \gamma$ that satisfy $1/\cos^2 \gamma = ||\mathbf{X}||^2$. The DAE inherits the pleasing feature of resources saving as in the previous work[26]. Moreover, the quantum counterparts of Eq.(2) and

Eq.(3) can be

$$\begin{aligned} \cos^{2p} \gamma f(\mathbf{X}) &= \frac{1}{2} \langle \mathbf{X} |^{\otimes p} A | \mathbf{X} \rangle^{\otimes p} \\ \cos^{2p-1} \gamma \hat{D}\mathbf{X} &= Tr_{p-1}[\rho_{\mathbf{X}}^{\otimes p-1} \mathcal{M}] |\mathbf{X}\rangle = \mathcal{D} |\mathbf{X}\rangle \end{aligned} \quad (5)$$

where $\rho_{\mathbf{X}} = |\mathbf{X}\rangle \langle \mathbf{X}|$ and $\mathcal{M} = \sum_{k=1}^p P_k A P_k$. Therefore, the iterative process of the gradient-based method is implemented as

$$|\mathbf{X}'\rangle = \cos \gamma' (|0\rangle + \sum_{i=1}^d x'_i |i\rangle) \propto |\mathbf{X}\rangle \pm \xi \mathcal{K} \mathcal{D} |\mathbf{X}\rangle, \quad (6)$$

This equation implies that $\cos \gamma^{2p-2}$ is absorbed into ξ , as the adjustable learning rate. Besides, the non-unitary operator $\mathcal{K} = \text{diag}(0, 1, 1, \dots, 1)$ is introduced after the application of \mathcal{D} , discarding the $|0\rangle$ component in $\mathcal{D} |\mathbf{X}\rangle$ and avoiding a trapped fake optimized state $|\mathbf{X}^{trap}\rangle$, which satisfies $\mathcal{D} |\mathbf{X}^{trap}\rangle \propto |\mathbf{X}^{trap}\rangle$. In this way, the final optimized $|\mathbf{X}^{op}\rangle$ is obtained and $\cos \gamma^{op}$ can be estimated within relative error ϵ_γ by consuming of $\mathcal{O}(\epsilon_\gamma^2)$ copies of this final states[30]. Hence, classical results can be got by reversing the DAE.

Noticeably, the combination of DAE and \mathcal{K} provides an alternative way to calculate the gradient of a general polynomials, varying from the previous work dealing with constrained homogeneous optimization. As some constrained optimization problems can be transformed into unconstrained optimization problems by introducing penalty function or Lagrange method, it extends the framework to more optimization cases.

Circuit—Circuit to implement Eq.(6) is specified in (Fig.1). It consists of three stages (divided by dashed lines), including four subroutines(colored), where, the *blue* block denotes the initialization of the input, the *pink* one denotes the construction of variable dependent \mathcal{D} , the *yellow* one denotes the construction of $e^{-i\mathcal{D}t}$ and the *green* one denotes the construction of \mathcal{K} . In details, the last three block are realized with the assistance of the qPCA[21], *HHL-like methods*[20, 31] and *linear combinations of unitary operators*[32–35].

For implementation, 5 principle registers are required. Three are labeled as k, up, d with one-qubit, assisting the construction of \mathcal{K} , variable updating and \mathcal{D} . One with χ qubits serves as the storage for eigenvalues of \mathcal{D} (labeled as e). The final register with $\log(d+1)$ qubits is labeled as v , encoding the variable $|\mathbf{X}\rangle$. Besides, there are implicit requirements of $[m(p-1)+1]$ copies of $|\mathbf{X}\rangle$ for implementation of variable dependent $e^{-i\mathcal{D}t}$. All χ, m determined by wanted precision and will be specified later.

In the following, we present a sketch of the protocol. Complexity analysis, as well as the error analysis is also given thereafter with the reasonable assumptions.

Stage-1: Subroutine-1 (colored blue) is the main body of this stage which encodes the current variable \mathbf{X} as $|\mathbf{X}\rangle_v$, i.e.

$$|0\rangle_k |0\rangle_{up} |0\rangle_d |0\rangle_e |\mathbf{X}\rangle_v, \quad (7)$$

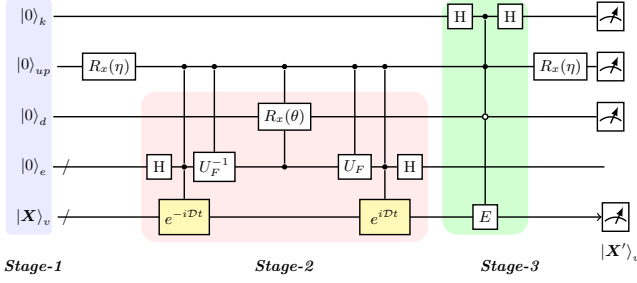


FIG. 1. Quantum circuit to implement the protocol, which consists of three stages (dashed lines) that evolving the system to the current iterative state. Four subroutines which implement initialization, non-unitary \mathcal{D} (by *HHL*-like methods), evolution $e^{-i\mathcal{D}t}$ (by *qPCA* and *Hamiltonian simulation* methods) and \mathcal{K} truncation are labeled in blue, pink, yellow and green in sequence.

Typically, the concerned optimal problems are usually insensitive to the initial variables. As is verified in numerical simulation, we can start with some easy-access states. Thus, the complexity of this subroutine can be ignored in the first iteration step. As for the following iterations, output of the former iteration can be used as the input. Even for a general \mathbf{X} , it can be realized via quantum random access memory (qRAM) [36, 37] or Hamiltonian simulation like method [38].

Therefore, a conservative estimate of *Subroutine-1* is admitted according to the qRAM or Hamiltonian simulation within $\mathcal{O}(\text{poly} \log d)$ time complexity [30].

Stage-2: a *HHL*-like subroutine (*Subroutine-2*) for implementing the non-unitary operation \mathcal{D} , and a *qPCA* & *Hamiltonian simulation* subroutine (*Subroutine-3*) for implementing the variable-dependent control evolution $C_{U_D} = \sum_{j=0}^{2^x-1} |j\rangle\langle j| e^{-i\mathcal{D} \frac{2\pi}{2^x} j}$, are involved in this part.

Local operation $R_{up}^x(\eta)$ is a preliminary treatment, which rotates $|0\rangle_{up}$ to $\cos \eta |0\rangle_{up} + \sin \eta |1\rangle_{up}$. Then a *HHL*-like method (colored pink) is implemented with the access to Hadamard gate H_e , controlled evolution C_{U_D} , controlled Fourier transform C_{U_F} and multi-controlled rotation $C_{R^x(\theta)}$, producing

$$\cos \eta |0\rangle_{up} |0\rangle_d |\mathbf{X}\rangle_v + \sin \eta |1\rangle_{up} (|0\rangle_d \mathcal{D} |\mathbf{X}\rangle + |1\rangle_d \mathcal{D}^\perp |\mathbf{X}\rangle) \quad (8)$$

where $\mathcal{D}^\perp |\mathbf{X}\rangle = \sum_k \sqrt{1 - \lambda_k^2} \beta_k |k\rangle$ and the register e is formatted via uncomputing.

On the premise that C_{U_D} is easy to realize, the complexity of this stage mainly comes from quantum phase estimation (qPE), which is specified in the standard textbook, requiring $\chi = n_p + \lceil \log(2 + \frac{1}{2\delta}) \rceil$ qubits and $\mathcal{O}(\chi^2)$ elemental gates. This guarantees a $1 - \delta$ success probability and bounded binary estimating error $\epsilon_p = 2^{-n_p}$. However, implementing C_{U_D} is nontrivial for its variable-dependence. We turn to *Subroutine-3* which integrates both qPCA method and Hamiltonian simulation. In this way, C_{U_D} is realized with a bounded error $\epsilon_D = \epsilon_{pca} + \epsilon_{hs}$. As to the circuit depth for C_{U_D} , it requires $\mathcal{O}(2p\pi s \|A\|_{max} + \frac{\log 1/\epsilon_{hs}}{\log \log 1/\epsilon_{hs}})$ queries on the coefficient oracles of A and $\mathcal{O}(4\pi^2 p^3 \|A\|_{max}^2 \log(1+d)/\epsilon_{pca})$ 2-qubit swap gates (s is the sparsity of A). With respect to the circuit size, it requires $\mathcal{O}(4\pi^2 p^3 \|A\|_{max}^2/\epsilon_{pca})$ copies for state $|\mathbf{X}\rangle$. Details on subroutines can be found in the Appendix [30].

Stage-3: For removing the $|0\rangle$ component in $\mathcal{D} |\mathbf{X}\rangle$ and avoiding 'tricky trap' states $|\mathbf{X}^{trap}\rangle$, the subroutine \mathcal{K} is implemented here, via a controlled operation $|0\rangle_k \langle 0| \otimes \mathbb{I}_{d+1} + |1\rangle_k \langle 1| \otimes E$ with $E = \text{diag}(-1, 1, 1, \dots, 1)$. Therefore, the full output state before $R_x(\eta)$ is

$$\cos \eta |0\rangle_k |0\rangle_{up} |0\rangle_d |\mathbf{X}\rangle + \sin \eta |0\rangle_k |1\rangle_{up} |0\rangle_d \mathcal{K} \mathcal{D} |\mathbf{X}\rangle + \sin \eta |0\rangle_k |1\rangle_{up} |1\rangle_d \mathcal{D}^\perp |\mathbf{X}\rangle + \sin \eta |1\rangle_k |1\rangle_{up} |0\rangle_d (\mathbb{I} - \mathcal{K}) \mathcal{D} |\mathbf{X}\rangle. \quad (9)$$

After $R_x(\mp \eta)$ and the post selection which is on the state $|0\rangle_k |0\rangle_{d_1} |0\rangle_{d_2}$ being applied, only the state

$$|\mathbf{X}'\rangle \propto \cos^2 \eta |\mathbf{X}\rangle \pm \sin^2 \eta \mathcal{K} \mathcal{D} |\mathbf{X}\rangle \quad (10)$$

is remained with a package error $\mathcal{E} = \epsilon_p + \epsilon_{pca} + \epsilon_{hs}$, which is the Eq.(6) with a tunable learning rate $\xi = \tan^2 \eta$.

The complexity of this stage comes from the implementation of \mathcal{K} , which requires $\mathcal{O}(\log(d+1))$ *Toffoli* gates and $\mathcal{O}(\log(d+1))$ extra qubits [30].

Success probability: In addition, the success probability of the each single iterative step with output $|\mathbf{X}'\rangle$ in Eq.(10) can be specified as

$$P_{succ} = \cos^4 \eta + \sin^4 \eta |\mathcal{K} \mathcal{D} |\mathbf{X}\rangle|^2 \pm \sin^2 \eta \cos^2 \eta (\langle \mathbf{X} | \mathcal{K} \mathcal{D} |\mathbf{X}\rangle + \langle \mathbf{X} | \mathcal{D} \mathcal{K} |\mathbf{X}\rangle) \quad (11)$$

Obviously, in the region $\xi = \tan^2 \eta \leq 1/2$, we have $P_{succ} \geq \cos^4 \eta - 2 \sin^2 \eta \cos^2 \eta$. That is, the success probability of each iteration can always be bounded finite by choosing of suitable ξ . For example, when we take $\xi = 1/3$, P_{succ} will always be larger than $3/16$.

Noticeably, success probability and multi-copies of the states $|\mathbf{X}\rangle$ used in *subroutine-3* may hinder the popularization of the protocol, as the memory utilization or the final success probability in slow-converging problem would bring disastrous impact to our devices and results. From this point of view, the number of iterations should be limited, i.e. a fast convergence problem is acceptable.

Simulation— To test the performance of our protocol, we explore two intuitionistic problems, including both maximum and minimum cases with corresponding

cost functions described as

$$\begin{aligned} \max \quad f_1 &= \frac{1}{2}(1, x)^{\otimes 2} A(1, x)^{T \otimes 2} \\ \min \quad f_2 &= \frac{1}{2}(1, x_1, x_2)^{\otimes 2} B(1, x_1, x_2)^{T \otimes 2} \end{aligned} \quad (12)$$

where A and B are coefficient matrix, which are specified in Appendix[30]. $x=4, 14$ (f_1) and $x=(\pm 5, \pm 5)$ (f_2) were set as the initial inputs. The system was driven by a circuit depicted in Fig.1 which includes at most 15 ancillary qubits($k=1, up=1, d=1, e \leq 12$). The simulation is gate-based with the assumption of accessible e^{iDt} . Thereby, the variable updates itself in compliance with Eq.(6) iteratively.

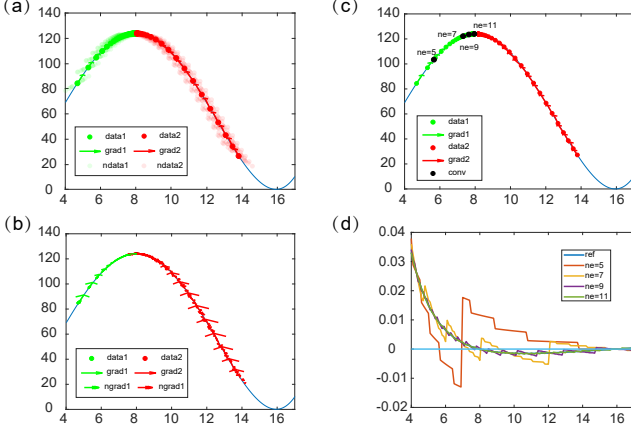


FIG. 2. Numerical simulation of 1-d optimization. Two projects with different initial trials are labeled in either green or red. Disturbance on the initial guess is shown in (a) with the iterations of the perturbed data(ndata1,ndata2). (b) shows imperfection of the gradient operator, with the slightly disturbed gradient, ngrad1 and ngrad2. (c) and (d) reveal the results of truncation errors from register e . With different sizes of register $e(n_e)$, the converging point(conv) varies as it encounter the zero-point of the gradient at the first time.

Results of simulation for optimizing f_1 and f_2 are represented in Fig.2 and Fig.3, in which 3 types errors are considered.(1)The initial error ϵ_I , coming from the imperfection of initialization, (2) the operation error ϵ_D , the imperfection when generating \mathcal{C}_{U_D} (In real situation, this comes from the *subroutine-3* caused by the defective Hamiltonian simulation or qPCA), and (3) the phase estimation error ϵ_{ph} for truncation caused by the size of register e .

Sub-figures (a) in Fig.2 and Fig.3 reveal the insensitive consequences of ϵ_I as the results hold unchanged while initial variables were sampled 20 times within 5% uniform random distribution around the setting values.

In sub-figures (b), to simulate the error ϵ_D , 1% and 5% random perturbations were applied to the \mathcal{D} for f_1 and f_2 , respectively. Obviously, a limited ϵ_D just leads to a slight deviation in both value and direction of the gradient, whose influence would be averaged as unstoppable it-

erations. However, This influence is problem-dependent. It depends on how close the different extreme points are. if the feasible region is complex, i.e. the different extreme points are too close or ϵ_D is comparably large, the iteration would get to fake extreme points with the stochastic perturbation. Anyway, in all likelihood, the correct optimal result would be finally obtained under a tolerable error ϵ_D .

Sub-figures (c) and (d) show the effects of ϵ_{ph} by the truncation in register e during the phase estimation. Generally, the size of register e determines the precision of the estimated eigenvalues $\{\lambda_k\}$ and thus the gradient operator. However, in practice, the sensitivity for the size of register e also depends on gradient value near the extreme points. For f_1 , the truncation error influences the point of convergence heavily as gradient varies slowly around 0, whose sign of \pm is easily switched. The black points in Fig.2(b) are the convergence points when the size of register $e(n_e)$ is 5,7,9,11, which indicates that we need choose at least $n_e = 12$ to get an acceptable result. On the other hand, for f_2 , the size of register e affects little to the position of the final result since gradient varies rapidly around the extreme point $(0, 0)$.

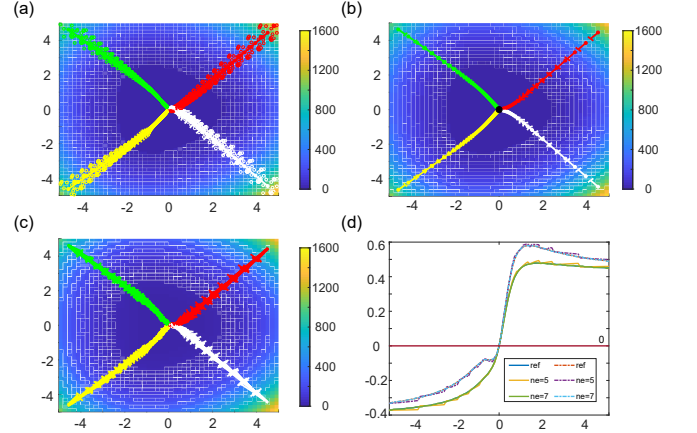


FIG. 3. Numerical simulation of 2-d minimum optimization. Four projects (white, yellow, green, red) are initialized with $\pm(5, 5)$, respectively. The insensitivity of the initial perturbation is shown in (a). The imperfectly implemented gradients, which is caused by ϵ_D , are displayed in (b). (c) unshrouds that the converging point stays although the different sizes of register $e(n_e)$, as a rapid climbing of the gradient around the extreme point, which is shown in (d).

DISCUSSION

In this paper, we propose an upgrade quantum gradient algorithm for general polynomial optimizations. With the DAE method and the non-unitary \mathcal{K} , it demolish the barrier of homogeneous of the cost function[26]. As constrained optimization problems usually can be

transformed into unconstrained optimization problems, our protocol, without the normalization constrain on argument, extends the framework to more optimization problems. Additionally, compared with the classical counterpart which costs $\mathcal{O}(d)$ operations and $\mathcal{O}(d)$ storage, the time consumption, as well as the memory utilization is reduced to $\mathcal{O}(\text{poly}(\log(d)))$ in its quantum version. Furthermore, numerical simulation was inspected with the noise and perturbation—initial error ϵ_I , operation error $\epsilon_{\mathcal{D}}$ and phase estimation error ϵ_{ph} . By the simulation results, the protocol shows its robustness to a tolerant errors, which is important for the real application in NISQ computers.

However, on a conservative estimation, every iteration the protocol costs multi-copies states due to Hamiltonian simulation and qPCA method. If the number of iterations required is unlimited, the protocol would be inefficient and unacceptable as the memory consumption grows exponentially. Besides, repeatedly run a probability algorithm would cause success probability decay exponentially. Therefore, only with fast convergence problems or with other combination methods which can get to the feasible region around converging point fast, our algorithm can perform efficiently in both memory and time consumption.

For modern day architectures, the number of optimized parameters would be at a level of billions. As the world become more and more intelligent, the field of the optimization which is the key to the machine-learning, especially in training the ML model whose objective function is polynomials, is requiring their heavy-lift to process more and more high-dimensional data. Although our protocol cannot give a clean answer to the optimization problem, even to a general polynomials, it is still significant for this field in certain cases. In the case when the feasible region is not comparably huge for the searching point, that means the iteration required is not too much, this quantum gradient method may provide exponential improvements over their classical counterparts.

Acknowledgements— K.L. acknowledge the National Natural Science Foundation of China under grant Nos. 11905111. P.G. J.G. S.W. and G.L. acknowledge the National Natural Science Foundation of China under Grants No. 11974205, and No. 11774197. The National Key Research and Development Program of China (2017YFA0303700); The Key Research and Development Program of Guangdong province (2018B030325002); Beijing Advanced Innovation Center for Future Chip (ICFC).

APPENDIX

CONTENTS

Introduction	1
Result	2
Discussion	4
Appendix	5
Gradient-based Algorithms	6
Framework of Quantum Gradient Descent Algorithm	6
Binary coding quantum algorithm	6
Amplitude coding quantum algorithm for even homogeneous polynomials	7
Subroutines	8
Subroutine-1: initialization	8
Subroutine-2: construction of D	8
Subroutine-3: Quantum principle component analysis	9
Subroutine-4: construction of \mathcal{K}	11
Hamiltonian simulation by quantum signal processing	11
Success probability	13
Algorithm Simulation	13

GRADIENT-BASED ALGORITHMS

Gradient algorithms, a first-order method, is widely applied in problems such as

$$\max_{\mathbf{x}} f(\mathbf{x}) \quad \text{or} \quad \min_{\mathbf{x}} f(\mathbf{x}), \quad \text{for all } \mathbf{x} \in \mathbb{R}^d, \quad (13)$$

where we confine the d -dimension variable \mathbf{x} to the real since the complex numbers can be processed with two independent real ones. Thus the problems can be solved iteratively with an iterative equation which is defined as

$$\mathbf{x}^{t+1} = \mathbf{x}^t \pm \xi \nabla f(\mathbf{x}^t), \quad (14)$$

where ξ is dubbed as the learning rate, the superscript t is labelled as the t -th step of iteration and $+$ ($-$) corresponds to the maximum(minimum) problems, respectively.

Various algorithms, derived from the prototypical gradient method, is playing an important role in nowadays machine-learning technology. Those gradient-based algorithms include first-order methods such as Vanilla, Stochastic, Mini-batch, Momentum, RMSprop and Adam methods, and the second-order methods such as Newton[8]. However, they are suffering the unmanageable consumption of either time or space for high-dimension parameter optimization since the typical gradient vector $\nabla f(\mathbf{x})$ in step t is usually approximated by a numerical differentiation methods as

$$\frac{\partial_i f(\mathbf{x})}{\partial x_i} \Big|_{\mathbf{x}^t} = \lim_{\delta \rightarrow 0} \frac{f(\cdots, x_i^t + \frac{\delta}{2}, \cdots) - f(\cdots, x_i^t - \frac{\delta}{2}, \cdots)}{\delta}. \quad (15)$$

This is known as symmetric difference quotient for discarding of second-order term and involves $2d$ times query of Oracle O_f which act as $O_f(\mathbf{x}) = f(\mathbf{x})$. So, when the variable dimension d grows larger and larger, especially being in billions for nowadays machine-learning, extremely high cost of time and space is required and the method is thus out of efficiency.

FRAMEWORK OF QUANTUM GRADIENT DESCENT ALGORITHM

Binary coding quantum algorithm

We review the framework of quantum gradient descent method proposed by Jordan, who encodes the variable in the binary from[22]

$$\mathbf{x}^t \rightarrow |\mathbf{x}^t\rangle = |x_1^t\rangle \otimes |x_2^t\rangle \otimes \cdots \otimes |x_d^t\rangle. \quad (16)$$

To assist the implementation of the gradient method, an Oracle U_f which act as

$$U_f : \quad U_f |\mathbf{x}^t\rangle = e^{i \frac{2\pi}{N_o} \frac{\eta}{2} f(\mathbf{x}^t)} |\mathbf{x}^t\rangle \quad (17)$$

is defined and could be realized by phase-kicking with ancilla qubits in state $|\psi\rangle = \frac{1}{\sqrt{2N_o/\eta}} \sum_{a=0}^{\frac{2N_o}{\eta}-1} e^{-i \frac{2\pi}{N_o} \frac{\eta}{2} a} |a\rangle$ as

$$\begin{aligned} & |\mathbf{x}^t\rangle \otimes |\psi\rangle \xrightarrow{f} |f(\mathbf{x}^t)\rangle \otimes |\psi\rangle \\ & \xrightarrow{C_{not}^{-1}} |f(\mathbf{x}^t)\rangle \otimes \frac{1}{\sqrt{2N_o/\eta}} \sum_{a=0}^{2N_o/\eta-1} e^{i \frac{2\pi}{N_o} \frac{\eta}{2} a} |a - f(\mathbf{x}^t)\rangle \\ & \xrightarrow{f^{-1}} e^{i \frac{2\pi}{N_o} \frac{\eta}{2} f(\mathbf{x}^t)} |\mathbf{x}^t\rangle \otimes |\psi\rangle \end{aligned} \quad (18)$$

And also, many other type modular addition can be done by modified control-Not gates, that is, phase kicking is a flexible method which is generally used to exponentiate binary numbers as phase value in quantum computation

world. With the hand of those, the full algorithm is given conditionally on the ancillary qubits as

$$\begin{aligned}
& \text{initial} : |\mathbf{x}^t\rangle \otimes |0\rangle \\
& \xrightarrow{\text{Hardmard}} \sum_{\delta} |\mathbf{x}^t\rangle \otimes |\delta\rangle \\
& \xrightarrow{C_{not}} \sum_{\delta} |\mathbf{x}^t + \xi\delta\rangle \otimes |\delta\rangle \\
& \xrightarrow{U_f} \sum_{\delta} e^{i\frac{2\pi}{N_0}\frac{\eta}{2}f(\mathbf{x}^t+\xi\delta)} |\mathbf{x}^t + \xi\delta\rangle \otimes |\delta\rangle \\
& \xrightarrow{cnot^{-2}} \sum_{\delta} e^{i\frac{2\pi}{N_0}\frac{\eta}{2}f(\mathbf{x}^t+\xi\delta)} |\mathbf{x}^t - \xi\delta\rangle \otimes |\delta\rangle \\
& \xrightarrow{U_f^{-1}} \sum_{\delta} e^{i\frac{2\pi}{N_0}\frac{\eta}{2}[f(\mathbf{x}^t+\xi\delta)-f(\mathbf{x}^t-\xi\delta)]} |\mathbf{x}^t - \xi\delta\rangle \otimes |\delta\rangle \\
& \xrightarrow{cnot} \sum_{\delta} e^{i\frac{2\pi}{N_0}\eta\xi\delta\cdot\nabla f(\mathbf{x}^t)} |\mathbf{x}^t\rangle |\delta\rangle \\
& = |\mathbf{x}^t\rangle |\eta\xi\nabla f(\mathbf{x}^t)\rangle \\
& \xrightarrow{cnot} |\mathbf{x}^t + \eta\xi\nabla f(\mathbf{x}^t)\rangle |\eta\xi\nabla f(\mathbf{x}^t)\rangle
\end{aligned} \tag{19}$$

where η scales the step size while ξ should be small enough for efficiency approximation of the gradient and mitigating the effect from non-linear term.

Bit-consumption is exactly the same as the classical methods. To preserve a d -dimension real variable to an accuracy $2^{-\chi}$, $d\chi$ qubits are required. As for the gate complexity, $O(d + \log_2 d)$ quantum gates are required from quantum Fourier transformation, just maintaining a same level as the classical algorithm. However, query complexity is reduced to only 2 for calling oracle O_f while $2d$ queries are needed in classical situation.

Amplitude coding quantum algorithm for even homogeneous polynomials

Variables are usually encoded as qubit-amplitude in quantum information processing for resources reduction and speed up. Rebentrost et al, absorbed it in their original quantum gradient descent work, which dealing with $2p$ -order homogeneous polynomials[26]. This optimization problem of homogeneous polynomials can be expressed in tensor language as

$$\begin{aligned}
f(\mathbf{x}^t) &= \sum_{m_1+\dots+m_d=2p} a_{m_1,\dots,m_d} (x_1^t)^{m_1} \dots (x_d^t)^{m_d} \\
&= \frac{1}{2} \mathbf{x}^{T\otimes} A \mathbf{x}^{\otimes p} \\
&= \frac{1}{2} \sum_{\alpha=1}^K \prod_{n=1}^p (\mathbf{x}^t)^T A_n^{\alpha} \mathbf{x}^t
\end{aligned} \tag{20}$$

where a_{m_1,\dots,m_d} is the coefficient of polynomials f and $\mathbf{x}^t = (x_1^t, x_2^t, \dots, x_d^t)^T$ is the multi-dimension variable. By involving the coefficients in a matrix $A_{d^p \times d^p}$, f can be seen as matrix product in conjugate of A and multi-folder vector $\mathbf{x}^{\otimes p}$, as in the second line in Eq.(20). A can always be chosen be real symmetric and composed of a sum of tensor product of unitary matrices $A = \sum_{\alpha=1}^K (\otimes_{n=1}^p A_n^{\alpha})$, where A_n^{α} acts on the n -th d -dimension variable space.

With above depiction, the gradient of $f(\mathbf{x}^t)$ can be explicitly determined by the current position \mathbf{x}^t

$$\nabla f(\mathbf{x}) = \sum_{\alpha=1}^K \sum_{n_1=1}^p A_{n_1}^{\alpha} \mathbf{x}^t \prod_{n_2=1, n_2 \neq n_1}^p (\mathbf{x}^t)^T A_{n_2}^{\alpha} \mathbf{x}^t \tag{21}$$

and the corresponding quantum amplitude encoding expressed as

$$\mathbf{x}^t = (x_1^t, x_2^t, \dots, x_d^t)^T \rightarrow |x\rangle^t = \sum_{i=1}^d x_i^t |i\rangle, \tag{22}$$

which implies the normalization constraint $\|\mathbf{x}^t\| = 1$. That is, the variable is constrained on a d -dimension sphere. It benefits the case where the results need not to be expressed explicitly but only used for further analysis, such as expectation value of some certain observables. In this way, the objective function as expectation value and gradient state can be rewritten as

$$f(\mathbf{x}^t) = \frac{1}{2} \sum_{\alpha=1}^K \prod_{n=1}^p \langle \mathbf{x}^t | A_n^\alpha | \mathbf{x}^t \rangle \quad (23)$$

$$|\nabla f(\mathbf{x}^t)\rangle_\alpha \propto \sum_{\alpha=1}^K \sum_{n_1=1}^p \prod_{\substack{n_2=1, \\ n_2 \neq n_1}}^p \langle \mathbf{x}^t | A_{n_2}^\alpha | \mathbf{x}^t \rangle A_{n_1}^\alpha | \mathbf{x}^t \rangle = \mathcal{D}_{\mathbf{x}^t} | \mathbf{x}^t \rangle \quad (24)$$

The key to obtain the iterative state is to apply the operator $\mathcal{D}_{\mathbf{x}^t}$ to the current state. Generally, it is a position-dependent operator which could be unitary or not. With the help of *Hamiltonian simulation*, *qPCA* and *HHL*-like methods at a cost of extra multi-copies of $|\mathbf{x}^t\rangle$, this operator application can be achieved as shown latter.

However, multi-copies state are required in each iteration, algorithm complexity would scale exponentially in the number of iterations steps performed. On the other hand, amplitude encoding may perform better in resources consumption, as the memory consumption is $O((poly(p) \log d)^{n_0})$, where n_0 is the number of iterations. In cases where a reasonable solution can be obtained with a limited iteration, it is acceptable for the memory consumption with $O(poly \log d)$. As for the gates complexity or query complexity, we leave them in our following work and analyze them as comparison.

In a word, for this method, the resources consumption scales logarithmically with variable dimension d and exponentially with iteration steps. Thus, it performs well with large d and fast-convergence problems.

SUBROUTINES

After inspecting the three stages in our algorithm in the main text, four stubborn problems are left to four subroutines. Here, we will show the corresponding details explicitly, including *Subroutine-1*, for initialization of the quantum register; *Subroutine-2*, for applying the *HHL*-like method; *Subroutine-3*, for implementing the variable-dependent $e^{-i\mathcal{D}}$ with quantum principle component analysis method and *Subroutine-4*, for constructing the Non-Unitary operation \mathcal{K} . In this section, we have drop the *step*-subscript or -superscript such as t and $_t$, and the *variable*-subscript $|\mathbf{x}\rangle$ for convenience.

Subroutine-1: initialization

Subroutine-1 serves as an operator, which drives the formatted variable register v to the current variable state $|\mathbf{X}\rangle = \cos \gamma(|0\rangle + \sum_{i=1}^d x_i |i\rangle)$. Typically, the concerned optimal problems are usually insensitive to the initial variables, so we can start with some product state, eg., $|0\rangle^{\otimes \log(d+1)}$. Thus, the complexity of this subroutine can be ignored in the first iteration step. As for the following iterations, output of the last iteration can play the role of this subroutine.

Even in some cases where we have to start with some particular state $|\psi\rangle$, the recent-published result shows only $\mathcal{O}(poly \log d)$ times of quantum manipulations are required with the help of 'bucket brigade' architecture of quantum random access memory(qRAM) per memory call[36?]. An alternative way that based on Grover search can also generate arbitrary quantum state with suitably bounded amplitude with fidelity nearly to 1 by consuming $\mathcal{O}(poly \log d)$ qubits[?]. Hence a conservative estimate of *Subroutine-1* is admitted within $\mathcal{O}(poly \log d)$ time complexity with error assumed as ϵ_I in this process.

Subroutine-2: construction of D

There are two quantum phase estimation modules and one double control operation in *Subroutine-2*. Suppose we have accessible controlled-unitary operation $C_{U_D} = |1\rangle\langle 1| \otimes \sum_{j=0}^{2^x-1} |j\rangle\langle j| e^{-i\frac{2\pi}{2^x} D j} + |0\rangle\langle 0| \otimes \mathbb{I}$ (whose implementation

will be specified in the next *Subroutine-3*), non-unitary operation \mathcal{D} can usually be constructed by a *HHL*-like method. After a single qubit rotation on register *up* which functions as

$$|0\rangle_{up} |0\rangle_d |0\rangle_e |\mathbf{X}\rangle_v \xrightarrow{R_{up}^x(\eta)} (\cos \eta |0\rangle_d + \sin \eta |1\rangle_{up}) |0\rangle_d |0\rangle_e |\mathbf{X}\rangle_v, \quad (25)$$

this method is sketched with the following derivation.

First, the binary estimation of the eigenvalues of \mathcal{D} can be resolved as λ_k (with corresponding eigenstate $|k\rangle$) to the eigenstate register *e* by quantum phase estimation method. The Hadamard gates H_e , control unitary evolution $C_{\mathcal{U}_D}$ and controlled quantum Fourier transformation on *e*, $C_{\mathcal{U}_F^{-1}}$ (functioned at state $|1\rangle_{up}$) are employed here in sequence. We summarize this procedure as

$$\begin{aligned} & \xrightarrow{H_e} \frac{1}{\sqrt{2^\chi}} (\cos \eta |0\rangle_{up} + \sin \eta |1\rangle_{up}) |0\rangle_d \sum_{j=0}^{2^\chi-1} |j\rangle_e |\mathbf{X}\rangle_v \\ & \xrightarrow{C_{\mathcal{U}_D}} \frac{\cos \eta}{\sqrt{2^\chi}} |0\rangle_{up} |0\rangle_d \sum_{j=0}^{2^\chi-1} |j\rangle_e |\mathbf{X}\rangle_v + \frac{\sin \eta}{\sqrt{2^\chi}} |1\rangle_{up} |0\rangle_d \sum_{k=1}^{d+1} \sum_{j=0}^{2^\chi-1} |j\rangle_e e^{-i\frac{2\pi}{2^\chi} \lambda_k j} \beta_k |k\rangle_v \\ & \xrightarrow{C_{\mathcal{U}_F^{-1}}} \frac{\cos \eta}{\sqrt{2^\chi}} |0\rangle_{up} |0\rangle_d \sum_{j=0}^{2^\chi-1} |j\rangle_e |\mathbf{X}\rangle_v + \frac{\sin \eta}{\sqrt{2^\chi}} |1\rangle_{up} |0\rangle_d \sum_{k=1}^{d+1} |\lambda_k\rangle_e \beta_k |k\rangle_v \end{aligned} \quad (26)$$

Then, a multi-control rotation depends on both register *up* and *e*, with angle $\theta = \arccos \lambda_k$ is applied on register *d*.

$$\xrightarrow{C_{R^x(\theta)}} \frac{\cos \eta}{\sqrt{2^\chi}} |0\rangle_{up} |0\rangle_d \sum_{j=0}^{2^\chi-1} |j\rangle_e |\mathbf{X}\rangle_v + \frac{\sin \eta}{\sqrt{2^\chi}} |1\rangle_{up} \sum_{k=1}^{d+1} (\lambda_k |0\rangle_d + \sqrt{1 - \lambda_k^2} |1\rangle_d) |\lambda_k\rangle_e \beta_k |k\rangle_v \quad (27)$$

Finally, the inverse conditional phase estimation procedure is conducted and the register *e* is uncoupled from the working system.

$$\begin{aligned} & \xrightarrow{C_{\mathcal{U}_F}} \frac{\cos \eta}{\sqrt{2^\chi}} |0\rangle_{up} |0\rangle_d \sum_{j=0}^{2^\chi-1} |j\rangle_e |\mathbf{X}\rangle_v + \frac{\sin \eta}{\sqrt{2^\chi}} |1\rangle_{up} \sum_{k=1}^{d+1} (\lambda_k |0\rangle_d + \sqrt{1 - \lambda_k^2} |1\rangle_d) \sum_{j=0}^{2^\chi-1} |j\rangle_e e^{-i\frac{2\pi}{2^\chi} \lambda_k j} \beta_k |k\rangle_v \\ & \xrightarrow{H_e \cdot C_{\mathcal{U}_D}^{-1}} \cos \eta |0\rangle_{up} |0\rangle_d |0\rangle_e |\mathbf{X}\rangle_v + \sin \eta |1\rangle_{up} \sum_{k=1}^{d+1} (\lambda_k |0\rangle_d + \sqrt{1 - \lambda_k^2} |1\rangle_d) |0\rangle_e \beta_k |k\rangle_v \end{aligned} \quad (28)$$

A following rotation $R_{d_1}^x(\eta)$ (or its inverse $(R_{up}^x(\eta))^{-1}$) on register *up* with post selection of $|0\rangle_{up} |0\rangle_d$ will reduce the result above to be effective $\frac{1}{N} (|\mathbf{X}\rangle_v - \tan^2 \eta \mathcal{D} |\mathbf{X}\rangle_v)$ (or $\frac{1}{N} (|\mathbf{X}\rangle_v + \tan^2 \eta \mathcal{D} |\mathbf{X}\rangle_v)$), that is, the corresponding update of gradient descent (or ascent). To be noticed that for the symmetry of this subroutine, all the operation dependency on register *up* except $C_{R^x(\theta)}$ in eq.(27) can be omitted with the result unchanged, thus it will make a more flexible realization.

When we talk about the complexity, you will find that $C_{R^x(\theta)}$ can be implemented within χ two-qubit control rotations. So, with the available $C_{\mathcal{U}_D}$ (the complexity of whose implementation will be discussed in the next subroutine), remaining resources consuming of this subroutine comes from standard *phase estimation* shown as,

Memory utilization

$$\chi = n_p + \lceil \log(2 + \frac{1}{2\delta_P}) \rceil \quad (29)$$

qubits are required for binary storing of $\{\lambda_k\}$ with accuracy $\epsilon_p = 2^{-n_p}$ and lower bound successful probability $1 - \delta_P$.

Time consumption

$$\mathcal{O}(\chi^2) \text{ gates} \quad (30)$$

Subroutine-3: Quantum principle component analysis

In this subroutine, we show that the variable dependent operator $\sum_{j=0}^{2^\chi-1} |j\rangle \langle j| e^{-i\mathcal{D} \frac{2\pi}{2^\chi} j}$ can be efficiently implemented within error ϵ_D by *Quantum Principle Component Analysis (qPCA)* methods.

First of all, we denote

$$\mathcal{M} = \sum_{k=1}^p P_k A P_k^\dagger = \sum_{\alpha=1}^K \sum_{n_1=1}^p A_{n_1}^\alpha \otimes \left(\bigotimes_{\substack{n_2=1, \\ n_2 \neq n_1}}^p A_{n_2}^\alpha \right) \quad (31)$$

and $\rho = |\mathbf{X}\rangle\langle\mathbf{X}|$, where P_k be the permutation between the 1-st and k -th subsystem.

By simple derivation of $qPCA$ process, one can find that τ -time evolution of the variable dependent gradient operator $\mathcal{D} = \text{Tr}_{p-1}[\rho^p \mathcal{M}]$ (the partial trace operated on the $p-1$ subsystem except the first one) can be approximated as

$$\begin{aligned} & \underbrace{\text{Tr}_{p-1} \left[e^{-i\mathcal{M}\frac{\tau}{m}} \rho^{\otimes p-1} \text{Tr}_{p-1} \left[e^{-i\mathcal{M}\frac{\tau}{m}} \rho^{\otimes p-1} \dots \text{Tr}_{p-1} \left[e^{-i\mathcal{M}\frac{\tau}{m}} \rho^{\otimes p} e^{i\mathcal{M}\frac{\tau}{m}} \right] \dots e^{i\mathcal{M}\frac{\tau}{m}} \right] e^{i\mathcal{M}\frac{\tau}{m}} \right]}_{m\text{-Trace}} \\ &= (e^{-i\mathcal{D}\frac{\tau}{m}})^m \rho (e^{i\mathcal{D}\frac{\tau}{m}})^m + \mathcal{O}(m \|\mathcal{D}\|_{max}^2 \frac{\tau^2}{m^2}) \\ &= e^{-i\mathcal{D}\tau} \rho e^{i\mathcal{D}\tau} + \mathcal{O}\left(\frac{p^2 \|\mathcal{A}\|_{max}^2 \tau^2}{m}\right) \end{aligned} \quad (32)$$

In a further step, $e^{-i\mathcal{M}\frac{\tau}{m}} = \prod_{k=1}^p P_k e^{-iA\frac{\tau}{m}} P_k + \mathcal{O}(\frac{p^2 \|\mathcal{A}\|_{max}^2 \tau^2}{m^2})$ (exactly the same error as in eq.(32), thus can be merged into each other latter) and $e^{-iA\frac{\tau}{m}}$ can be easily constructed with only access to the coefficient matrix A , that is, the well known two oracles

Oracle 1: $O_1 |j, k\rangle |0\rangle = |j, k\rangle |A_{jk}\rangle$

Oracle 2: $O_2 |j, l\rangle = |j, k_A(j, l)\rangle$

where $k_A(j, l)$ denotes the column index of l -th nonzero element in A 's j -th row.

By the results of Childs' and Low's work[35?], one can efficient implement the sparse Hamiltonian simulation $e^{-iA\frac{\tau}{m}}$ with error $\tilde{\epsilon}$ within $\mathcal{O}(\frac{s\|\mathcal{A}\|_{max}\tau}{m} + \frac{\log 1/\tilde{\epsilon}}{\log \log 1/\tilde{\epsilon}})$ times queries of O_1 and O_2 , combined with $\mathcal{O}(p \log(d+1) + \chi' \text{poly} \log \chi')$ gates, where $2^{-\chi'}$ be the Binary accuracy of A 's element as specified in O_1 and s be A 's sparsity. The details can be find in next section and [35?]. So in a word, this shows that variable dependent $\mathcal{C}_{\mathcal{U}_D}$ can be implemented with the help of $qPCA$, *Hamiltonian simulation* and multi copies of states $\rho = |\mathbf{X}\rangle\langle\mathbf{X}|$. In the following, we will discuss about the corresponding complexity and operation errors.

Noticed that the control evolution $\mathcal{C}_{\mathcal{U}_D} = \sum_{j=0}^{2^x-1} |j\rangle\langle j| e^{-i\mathcal{D}\frac{2\pi}{2^x}j}$ can be constructed by Eq.(32) when $\mathcal{C}_{\mathcal{U}_A} = \sum_{j=0}^{2^x-1} |j\rangle\langle j| e^{-iA\frac{2\pi}{m2^x}j}$ takes the place of $e^{-iA\frac{\tau}{m}}$ as mentioned before. So once $\mathcal{C}_{\mathcal{U}_A}$ be available, we take $m = \frac{4\pi^2 p^2 \|\mathcal{A}\|_{max}}{\epsilon_{pca}}$ to bound the $qPCA$ induce error in $\mathcal{C}_{\mathcal{U}_D}$ as ϵ_{pca} . Meanwhile,

$$\mathcal{O}(mp) = \mathcal{O}\left(\frac{4\pi^2 p^3 \|\mathcal{A}\|_{max}^2}{\epsilon_{pca}}\right) \quad (33)$$

copies of state $\rho = |\mathbf{X}\rangle\langle\mathbf{X}|$ and

$$\mathcal{O}\left(\frac{4\pi^2 p^3 \|\mathcal{A}\|_{max}^2 \log(1+d)}{\epsilon_{pca}}\right) \quad (34)$$

two qubits swap gates(for implementation of P_k), required in this $qPCA$ process.

Besides, since the $\mathcal{C}_{\mathcal{U}_A}$ can be constructed as

$$\sum_{j=0}^{2^x-1} |j\rangle\langle j| e^{-iA\frac{2\pi}{m2^x}j} = \sum_{\{j_k=0,1\}} |j_1\rangle\langle j_1| e^{-iA\frac{2\pi}{m2}j_1} \dots |j_k\rangle\langle j_k| e^{-iA\frac{2\pi}{m2^k}j_k} \dots |j_x\rangle\langle j_x| e^{-iA\frac{2\pi}{m2^x}j_x} \quad (35)$$

and the Hamiltonian simulation complexity scales linearly with evolution time, usually in the case of limited ξ , the complexity in constructing $\mathcal{C}_{\mathcal{U}_A}$ contributes to the 1st term in Eq.35. We can easily find that mp times queries of $\mathcal{C}_{\mathcal{U}_A}$ share the same implementation complexity and Hamiltonian simulation induced error ϵ_{hs} with $e^{-iA\frac{2\pi}{m2^x}j}$, specifically, that is

$$\mathcal{O}(2p\pi s \|\mathcal{A}\|_{max} + \frac{\log 1/\epsilon_{hs}}{\log \log 1/\epsilon_{hs}}) \quad (36)$$

times queries of O_1 and O_2 .

In the last, the full error(both from *qPCA* and *Hamiltonian simulation*) of control evolution $\mathcal{C}_{\mathcal{U}_D}$ can be bounded by these two independent error as

$$\epsilon_{\mathcal{D}} = \epsilon_{pca} + \epsilon_{hs} \quad (37)$$

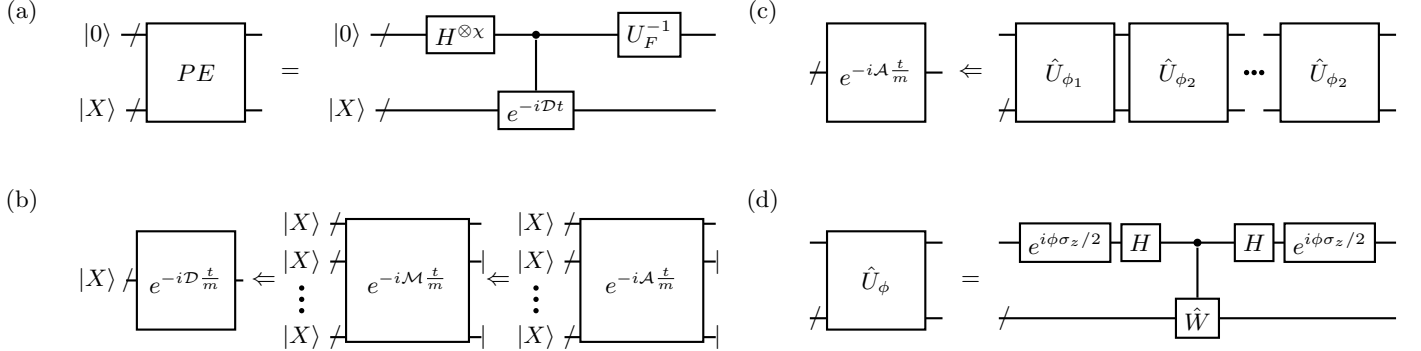


FIG. 4. The structure to implement the *subroutine-2*.(a) is the standard quantum phase estimation modular, where $e^{-iD\tau}$ can be simulated in (b), which simulate a piece of time τ/m with the *subroutine-3*, via the qCPA and Hamiltonian simulation of \mathcal{A} .(c) and (d) are the Hamiltonian simulation with quantum signal processing method by adding one ancillary qubit.

Subroutine-4: construction of \mathcal{K}

Recall that since there is a projection constraint $\|\mathbf{x}\| = 1$ in previous work[26], all variable lied in a high-dimension sphere and the iteration stopped at state $|\mathbf{x}\rangle \propto \mathcal{D}|\mathbf{x}\rangle$ since the projected gradient vanished.

However, as the projection constrained moved out in our work by the dressed amplitude encoding $\mathbf{x} \rightarrow |\mathbf{X}\rangle = \cos \gamma(|0\rangle + \sum_{i=1}^d |i\rangle)$, quantum state $|\mathbf{X}^{op}\rangle$ which satisfy $|\mathbf{X}^{op}\rangle \propto |\mathbf{X}^{op}\rangle - \mathcal{K}\mathcal{D}|\mathbf{X}^{op}\rangle$ be the new optimized result, instead of state $|\mathbf{X}^{trap}\rangle$ which satisfy $\mathcal{D}|\mathbf{X}^{trap}\rangle \propto |\mathbf{X}^{trap}\rangle$, where $\mathcal{K} = \text{diag}(0, 1, 1, \dots, 1)$.

Non-unitary \mathcal{K} can be well implemented with the help of one single ancilla qubit as

$$\mathcal{K}|\psi\rangle \propto |0\rangle_a \langle 0|_a H_a C_E H_a |0\rangle_a |\psi\rangle \quad (38)$$

where H_a be Hadamard and $C_E = |0\rangle_a \langle 0|_a \otimes \mathbb{I} + |1\rangle_a \langle 1|_a \otimes \text{diag}(-1, 1, 1, \dots, 1)$ (or in another view, $C_E = C_{Z_a}^0$, a control-Z gate on ancilla functioned when the principle system in state $|0\rangle$). The success probability of post selection on ancilla qubit state $|0\rangle$ equal to the weight of non- $|0\rangle$ component in $|\psi\rangle$, which match the applied condition of this optimal method, that is, the object function being fast converged (that is, with finite gradient).

Notice that $C_E = C_{Z_a}^0 = X^{\otimes \log(d+1)} C_{Z_a}^1 X^{\otimes \log(d+1)}$, where $C_{Z_a}^1$ can be easily implemented with $\mathcal{O}(\log(d+1))$ Toffoli gates and $\mathcal{O}(\log(d+1))$ extra qubits which set in $|0\rangle$ (or in another way, this can be done with $\mathcal{O}(\log^2(d+1))$ Toffoli gates without ancillary).

HAMILTONIAN SIMULATION BY QUANTUM SIGNAL PROCESSING

In this section, the method of quantum signal processing(QSP) to complete the evolution e^{-iHt} of d -dimension Hamiltonian H (where A play the role of H in *subroutine-3*) is introduced. This method is based on the sparse matrix assumption, which involves two oracles.

Oracle 1: $O_1 |j, k\rangle |0\rangle = |j, k\rangle |H_{jk}\rangle$

Oracle 2: $O_2 |j, l\rangle = |j, k_H(j, l)\rangle$

where polynomial coefficients oracle O_1 operates on $\chi' + 2 \log(d)$ qubits with $i, j = 1, \dots, d$, to hold an accuracy of H 's elements to $2^{-\chi'}$. The function $k_H(j, l)$ output the column index of l -th nonzero element in j -th row of H . Sparse input oracle O_2 operates on $2 \log d$ qubits and $l = 1, \dots, s$, where s just be the sparsity of H .

The result shows one can efficient implement the sparse- s Hamiltonian simulation e^{-iHt} with error ϵ_{hs} within

Query complexity: $\mathcal{O}(s\|H\|_{max}t + \frac{\log 1/\epsilon_{hs}}{\log \log 1/\epsilon_{hs}})$

Gate complexity: $\mathcal{O}(\log d + \chi' poly \log \chi')$

In the following, we will sketch the QSP for Hamiltonian simulation. Fig.4 (c) and (d) give the basic idea. Both circuits consist of two input, one ancillary qubit and a workspace. A series of \hat{U}_ϕ build up our simulation circuit, where \hat{U}_ϕ (shown in Fig.4) consists of the Hadamard gates, z -rotations and controlled- \hat{W} operation. when the system input is on the eigenvectors $|\lambda\rangle$, i.e. $\hat{W}|\lambda\rangle = e^{i\theta_\lambda}|\lambda\rangle$, it can be reduced to the single-qubit rotation $R_\phi(\theta_\lambda)$ on the ancilla, where $R_\phi(\theta_\lambda) = e^{-i(\theta_\lambda/2)(\sigma_x \cos(\phi) + \sigma_y \sin(\phi))}$.

A general $e^{ih(\theta_\lambda)}$ can be approximated with $R_{\phi_1}(\theta_\lambda)R_{\phi_2}(\theta_\lambda)\dots R_{\phi_n}(\theta_\lambda)$ via optimizing the parameters $\phi_1, \phi_2, \dots, \phi_n$ in the sequence of the \hat{U}_A (shown in the Fig.4(c)), which builds up a transformation on the functional workspace

$$\begin{aligned} W &= \sum_{\lambda} e^{i\theta_\lambda} |\lambda\rangle \langle \lambda| \\ \rightarrow V &= \sum_{\lambda} e^{ih(\theta_\lambda)} |\lambda\rangle \langle \lambda| \end{aligned} \quad (39)$$

When $h(\theta_\lambda) = -\tau \sin(\theta_\lambda)$, the simulation circuit can be used in the Hamiltonian simulation via quantum walk.

We will given a brief illustration on Hamiltonian simulation via QSP. Given a s -sparse Hamiltonian H acting on d dimension Hilbert space. First of all, an ancillary qubit with the state $|0\rangle$ is appended, expanding the space from d to $2d$, then the entire Hilbert space is duplicated (thus $\mathbb{C}^{2d} \otimes \mathbb{C}^{2d}$). The whole process can be done with the isometry T

$$T = \sum_{j=0}^{d-1} \sum_{b \in \{0,1\}} (|j\rangle \langle j| \otimes |b\rangle \langle b|) \otimes |\phi_{j,b}\rangle \quad (40)$$

where $|\phi_{j,0}\rangle$ and $|\phi_{j,1}\rangle$ are defined as

$$\begin{aligned} |\phi_{j,0}\rangle &= \frac{1}{\sqrt{s}} \sum_{l \in S_j} \left(|l\rangle \sqrt{\frac{H_{i,l}}{X}} |0\rangle + \sqrt{1 - \frac{|H_{i,l}^*|}{X}} |1\rangle \right) \\ |\phi_{j,1}\rangle &= |0\rangle |1\rangle \end{aligned} \quad (41)$$

with $X \geq \|H\|_{max}$ and S_j be the set of indices of nonzero elements in column j of H . This is a controlled state preparation step, performing on the input $|j\rangle|b\rangle$, to creat $|\phi_{j,b}\rangle (b=0,1)$. In the step, one query to the oracle O_1 and O_2 and additional $(\chi' ploy \log(\chi'))$ primitive gates are required. After this stage, the unitary operator of the quantum walk are applied with

$$U = iS(2TT^\dagger - \mathbb{I}) \quad (42)$$

S is swap operation, acting on the former and latter two register as $S|j_1\rangle|b_1\rangle|j_2\rangle|b_2\rangle = |j_2\rangle|b_2\rangle|j_1\rangle|b_1\rangle$ where $j_1, j_2 \in [d]$ and $b_1, b_2 \in \{0,1\}$. As U corresponds to reflection about TT^\dagger followed by S , swapping $(2 + 2 \log d)$ -qubit registers, its query and gate complexities are identical to T up to constant factors.

Suppose that $|\lambda\rangle$ be H 's eigenstates as $H|\lambda\rangle = \lambda|\lambda\rangle$, The quantum walk operator U and its eigenvalues μ_\pm thus satisfy the following rules

$$\begin{aligned} U|\mu_\pm\rangle &= \mu_\pm|\mu_\pm\rangle \\ |\mu_\pm\rangle &= (1 + i\mu_\pm S)T|\lambda\rangle, \mu_\pm = \pm e^{\pm i \arcsin(\lambda/Xs)} \end{aligned} \quad (43)$$

Since

$$\|T \frac{1-iS}{\sqrt{2}} (iU)^\tau \frac{1+iS}{\sqrt{2}} T^\dagger - e^{i\tau \sin^{-1}(H/\|abs(H)\|)}\| < (\|H\|/\|abs(H)\|)^2 \quad (44)$$

If λ/Xs is small enough, applying $\tau = s\|H\|_{max}t$ steps of the discrete-time quantum walk U , we could simulate t time Hamiltonian simulation since[34]. Therefore, finally, the inverse state preparation T^\dagger is performed. For a successful simulation, the output should lie in the original space, and the ancillary qubit should be returned to the state $|0\rangle$.

The hint is, the nonlinear of the phase factor $\arcsin(\lambda/Xs)$ making the simulation deviate from the desired value. The transformation via quantum signal processing from W to V is applied here, when $h(\theta_\lambda) = -\tau \sin(\theta_\lambda)$. It modifies the simulation circuit to a controlled one(the simulation circuit is just the W in above protocol).

SUCCESS PROBABILITY

By simple derivation, the full output state in circuits in main text before $R_x(\eta)$ acted can be shown as

$$\begin{aligned} & \cos \eta |0\rangle_k |0\rangle_{up} |0\rangle_d |\mathbf{X}\rangle + \sin \eta |0\rangle_k |1\rangle_{up} |0\rangle_d \mathcal{K} \mathcal{D} |\mathbf{X}\rangle \\ & + \sin \eta |0\rangle_k |1\rangle_{up} |1\rangle_d \mathcal{D}^\perp |\mathbf{X}\rangle + \sin \eta |1\rangle_k |1\rangle_{up} |0\rangle_d (\mathbb{I} - \mathcal{K}) \mathcal{D} |\mathbf{X}\rangle \end{aligned} \quad (45)$$

where $\mathcal{D}^\perp |\mathbf{X}\rangle$ denotes the rubbish state $\sum_k \sqrt{1 - \lambda_k^2} \beta_k |k\rangle$. Obviously, when $R_x(\mp \eta)$ applied and post selected on state $|0\rangle_k |0\rangle_{d1} |0\rangle_{d2}$, only the

$$\cos^2 \eta |\mathbf{X}\rangle \pm \sin^2 \eta \mathcal{K} \mathcal{D} |\mathbf{X}\rangle \quad (46)$$

preserved, with probability

$$P_{succ} = \cos^4 \eta + \sin^4 \eta |\mathcal{K} \mathcal{D} |\mathbf{X}\rangle|^2 \pm \sin^2 \eta \cos^2 \eta (\langle \mathbf{X} | \mathcal{K} \mathcal{D} | \mathbf{X} \rangle + \langle \mathbf{X} | \mathcal{D} \mathcal{K} | \mathbf{X} \rangle) \quad (47)$$

Typically, when the tunable learning rate $\xi = \tan^2 \eta$ chosen to be less than 1/2, we have

$$P_{succ} \geq \cos^4 \eta - 2 \sin^2 \eta \cos^2 \eta. \quad (48)$$

for both descent and ascent cases. That is, the success probability of each iteration can always be bounded as finite by choosing of suitable $\xi(\eta)$. For example, when we take $\xi = 1/3$, P_{succ} will always be larger than 3/16.

ALGORITHM SIMULATION

Based on the theoretical protocol, the simulation program consists of an iteration of three stages as depicted in the article. The program assumed that the Hamiltonian simulation, i.e. e^{iDt} can be simulated directly in the machine. Therefore, two cases are simulated in the frame of our protocol.

The polynomial optimizations include both maximum and minimum problems, which state as

$$\begin{aligned} \max \quad & f_1 = \frac{1}{2} (1, x)^{\otimes 2} \begin{pmatrix} 7/2 & 0 \\ 0 & -9/2 \end{pmatrix}^{\otimes 2} (1, x)^{T \otimes 2} \\ \min \quad & f_2 = \frac{1}{2} (1, x_1, x_2)^{\otimes 2} \left[\begin{pmatrix} 1 & 0 & 0 \\ 0 & 1 & 0 \\ 0 & 0 & 1 \end{pmatrix}^{\otimes 2} + \begin{pmatrix} 0 & 0 & 1 \\ 0 & 0 & 0 \\ 1 & 0 & 0 \end{pmatrix} \otimes \begin{pmatrix} 0 & 0 & 0 \\ 0 & 0 & 1 \\ 0 & 1 & 0 \end{pmatrix} \right] (1, x_1, x_2)^{T \otimes 2} \end{aligned} \quad (49)$$

According to the protocol, an arbitrary initial input $(1, \mathbf{x}')$ can be represented with DAE by a quantum state $|\mathbf{X}\rangle = \cos \gamma (|0\rangle + \sum_i x_i |i\rangle)$. All projects are based on the circuit model, which consists of a set of elementary quantum gates, i.e. arbitrary single-qubit rotations and two-qubit controlled-unitary operators.

Initialization was implemented by the rotations on a qubit or a qutrit, as measurement was realized by simulating tomography on the variable register e , after projecting entire system into the target subspace. As for the intermediate procedures, the gates are implemented as the algorithm circuit with the assumption to get e^{iDt} .

Remarkably, the standard phase estimation module approximates the eigenvalue of the target unitary with a range of $(0, 1)$. However, this module should be modified since when constructing the D , the gradient operator produces both the positive and negative component. The periodic property is utilized in our implementation and the eigenvalues in the gradient operator are normalized in a range of $(-\frac{1}{2}, \frac{1}{2})$. Therefore, the output of this module is divided into two parts, results in $(0, \frac{1}{2})$ is directly readout while others in $(\frac{1}{2}, 1)$ should be resolved into the range of $(-\frac{1}{2}, 0)$ by the periodic condition.

In the program, the simulation includes 15 ancillary qubit in a conservative way, with 1 for k , 1 for $d1$, 1 for $d2$ and 12 for e , whose resolution has been discussed in article. The rest qubits are used to encode the variables. During the simulation, $\mathbf{x} = (1, 7 \pm 3)$ are considered as the two random initial guess for f_1 , and $\mathbf{x} = (1, \pm 5, \pm 5)$ are chosen as four different initial variables for f_2 . And 0.05(0.1) is chosen as the learning rate for f_1 (f_2).

3 types errors are investigated, including the initial error ϵ_I , the operation error ϵ_D and the phase estimation error ϵ_{ph} . ϵ_I comes from the imperfection of initialization which cannot arrive at the target input. we simulate this situation repeatably for 20 times, by introducing a perturbation with uniform random distribution whose amplitude is 5% to the input state. ϵ_D is from the uncertainty of the e^{iDt} , as e^{iDt} cannot be perfectly generated. We introduced the noise into the operator, with 1% and 2% to the amplitude of D for two cases, and simulated them for 15 times. ϵ_{ph}

is the truncation error which originated from the size of eigenvalue register e . To simulate this situation, we choose different sizes of the e for 5,7,9,11. On the other side, we investigate the effects on gradient value of different sizes of e .

* These authors contributed equally to this work.

† gllong@tsinghua.edu.cn

- [1] Lei Wang. Discovering phase transitions with unsupervised learning. *Physical Review B*, 94(19):195105, 2016.
- [2] Evert PL Van Nieuwenburg, Ye-Hua Liu, and Sebastian D Huber. Learning phase transitions by confusion. *Nature Physics*, 13(5):435–439, 2017.
- [3] Giuseppe Carleo and Matthias Troyer. Solving the quantum many-body problem with artificial neural networks. *Science*, 355(6325):602–606, 2017.
- [4] Ulrich Schollwck. The density-matrix renormalization group in the age of matrix product states. *Annals of Physics*, 326(1):96–192, 2011.
- [5] Dong-Ling Deng, Xiaopeng Li, and S Das Sarma. Quantum entanglement in neural network states. *Physical Review X*, 7(2):021021, 2017.
- [6] Yoav Levine, Or Sharir, Nadav Cohen, and Amnon Shashua. Quantum entanglement in deep learning architectures. *Physical review letters*, 122(6):065301, 2019.
- [7] Giacomo Torlai, Guglielmo Mazzola, Juan Carrasquilla, Matthias Troyer, Roger Melko, and Giuseppe Carleo. Neural-network quantum state tomography. *Nature Physics*, 14(5):447–450, 2018.
- [8] Jiawei Zhang. Gradient descent based optimization algorithms for deep learning models training. *arXiv preprint arXiv:1903.03614*, 2019.
- [9] Gunasekaran Manogaran and Daphne Lopez. Health data analytics using scalable logistic regression with stochastic gradient descent. *International Journal of Advanced Intelligence Paradigms*, 10(1-2):118–132, 2018.
- [10] Zhen Wang, Yuan-Hai Shao, Lan Bai, Chun-Na Li, Li-Ming Liu, and Nai-Yang Deng. Insensitive stochastic gradient twin support vector machines for large scale problems. *Information Sciences*, 462:114–131, 2018.
- [11] Simon S Du, Jason D Lee, Haochuan Li, Liwei Wang, and Xiyu Zhai. Gradient descent finds global minima of deep neural networks. *arXiv preprint arXiv:1811.03804*, 2018.
- [12] Yi Sun, Yuheng Chen, Xiaogang Wang, and Xiaoou Tang. Deep learning face representation by joint identification-verification. In *Advances in neural information processing systems*, pages 1988–1996, 1988–1996.
- [13] Francesco Ricci, Lior Rokach, and Bracha Shapira. *Introduction to recommender systems handbook*, pages 1–35. Springer, 2011.
- [14] Mariusz Bojarski, Davide Del Testa, Daniel Dworakowski, Bernhard Firner, Beat Flepp, Prashoon Goyal, Lawrence D Jackel, Mathew Monfort, Urs Muller, and Jiakai Zhang. End to end learning for self-driving cars. *arXiv preprint arXiv:1604.07316*, 2016.
- [15] Frank Arute, Kunal Arya, Ryan Babbush, Dave Bacon, Joseph C Bardin, Rami Barends, Rupak Biswas, Sergio Boixo, Fernando GSL Brandao, and David A Buell. Quantum supremacy using a programmable superconducting processor. *Nature*, 574(7779):505–510, 2019.
- [16] JM Pino, JM Dreiling, C Figgatt, JP Gaebler, SA Moses, CH Baldwin, M Foss-Feig, D Hayes, K Mayer, and C Ryan-Anderson. Demonstration of the qccd trapped-ion quantum computer architecture. *arXiv preprint arXiv:2003.01293*, 2020.
- [17] Michael A Nielsen and Isaac Chuang. *Quantum computation and quantum information*. American Association of Physics Teachers, 2002.
- [18] J. Biamonte, P. Wittek, N. Pancotti, P. Rebentrost, N. Wiebe, and S. Lloyd. Quantum machine learning. *Nature*, 549(7671):195–202, 2017.
- [19] Michael Broughton, Guillaume Verdon, Trevor McCourt, Antonio J Martinez, Jae Hyeon Yoo, Sergei V Isakov, Philip Massey, Murphy Yuezhen Niu, Ramin Halavati, and Evan Peters. Tensorflow quantum: A software framework for quantum machine learning. *arXiv preprint arXiv:2003.02989*, 2020.
- [20] A. W. Harrow, A. Hassidim, and S. Lloyd. Quantum algorithm for linear systems of equations. *Phys Rev Lett*, 103(15):150502, 2009.
- [21] Seth Lloyd, Masoud Mohseni, and Patrick Rebentrost. Quantum principal component analysis. *Nature Physics*, 10(9):631–633, 2014.
- [22] S. P. Jordan. Fast quantum algorithm for numerical gradient estimation. *Phys Rev Lett*, 95(5):050501, 2005.
- [23] Andrs Gilyn, Srinivasan Arunachalam, and Nathan Wiebe. Optimizing quantum optimization algorithms via faster quantum gradient computation. In *Proceedings of the Thirtieth Annual ACM-SIAM Symposium on Discrete Algorithms*, pages 1425–1444. SIAM, 2019.
- [24] Jun Li, Xiaodong Yang, Xinhua Peng, and Chang-Pu Sun. Hybrid quantum-classical approach to quantum optimal control. *Physical review letters*, 118(15):150503, 2017.
- [25] Maria Schuld, Ville Bergholm, Christian Gogolin, Josh Izaac, and Nathan Killoran. Evaluating analytic gradients on quantum hardware. *Physical Review A*, 99(3):032331, 2019.
- [26] Patrick Rebentrost, Maria Schuld, Leonard Wossnig, Francesco Petruccione, and Seth Lloyd. Quantum gradient descent and newtons method for constrained polynomial optimization. *New Journal of Physics*, 21(7), 2019.
- [27] Iordanis Kerenidis and Anupam Prakash. Quantum gradient descent for linear systems and least squares. *Physical Review A*, 101(2):022316, 2020.
- [28] Sung-Kwun Oh, Witold Pedrycz, and Byoung-Jun Park. Polynomial neural networks architecture: analysis and design. *Computers & Electrical Engineering*, 29(6):703–725, 2003.
- [29] Ladislav Zjavka. Wind speed forecast correction models using polynomial neural networks. *Renewable Energy*, 83:998–1006, 2015.
- [30] *See Supplemental Information for a detailed description of the theory.*
- [31] Shijie Wei, Zengrong Zhou, Dong Ruan, and Guilu Long. Realization of the algorithm for system of linear equations in duality quantum computing. In *vehicular technology conference*, pages 1–4, 2017.
- [32] Gui Lu Long. Duality quantum computing and duality

- quantum information processing. *International Journal of Theoretical Physics*, 50(4):1305–1318, 2011.
- [33] Shijie Wei, Hang Li, and Guilu Long. A full quantum eigensolver for quantum chemistry simulations. *Research*, 2020(1486935):11, 2020.
 - [34] Andrew M. Childs. On the relationship between continuous- and discrete-time quantum walk. *Communications in Mathematical Physics*, 294(2):581–603, 2009.
 - [35] Dominic W. Berry, Andrew M. Childs, and Robin Kothari. Hamiltonian simulation with nearly optimal dependence on all parameters. In *2015 IEEE 56th Annual Symposium on Foundations of Computer Science*, pages 792–809.
 - [36] V. Giovannetti, S. Lloyd, and L. Maccone. Quantum random access memory. *Phys Rev Lett*, 100(16):160501, 2008.
 - [37] Vittorio Giovannetti, Seth Lloyd, and Lorenzo Maccone. Architectures for a quantum random access memory. *Physical Review A*, 78(5), 2008.
 - [38] Leonard Wossnig, Zhikuan Zhao, and Anupam Prakash. Quantum linear system algorithm for dense matrices. *Physical review letters*, 120(5):050502, 2018.